Progress In Electromagnetics Research, Vol. 151, 127–150, 2015

Electromagnetic Field Transformations for Measurements and Simulations

Thomas F. Eibert*, Emre Kılıç, Carlos Lopez, Raimund A. M. Mauermayer, Ole Neitz, and Georg Schnattinger

(*Invited Paper*)

Abstract—Electromagnetic field transformations are important for electromagnetic simulations and for measurements. Especially for field measurements, the influence of the measurement probe must be considered, and this can be achieved by working with weighted field transformations. This paper is a review paper on weighted field transformations, where new information on algorithmic properties and new results are also included. Starting from the spatial domain weighted radiation integral involving free space Green's functions, properties such as uniqueness and the meaning of the weighting function are discussed. Several spectral domain formulations of the weighted field transformation integrals are reviewed. The focus of the paper is on hierarchical multilevel representations of irregular field transformations with propagating plane waves on the Ewald sphere. The resulting Fast Irregular Antenna Field Transformation Algorithm (FIAFTA) is a versatile and efficient transformation technique for arbitrary antenna and scattering fields. The fields can be sampled at arbitrary irregular locations and with arbitrary measurement probes without compromising the accuracy and the efficiency of the algorithm. FIAFTA supports different equivalent sources representations of the radiation or scattering object: 1) equivalent surface current densities discretized on triangular meshes, 2) plane wave representations, 3) spherical harmonics representations. The current densities provide for excellent spatial localization and deliver most diagnostics information about the test object. A priori information about the test object can easily be incorporated, too. Using plane wave and spherical harmonics representations, the spatial localization is not as good as with spatial current densities, but still much better than in the case of conventional modal expansions. Both far-field based expansions lead to faster transformations than the equivalent currents and in particular the orthogonal spherical harmonics expansion is a very attractive and robust choice. All three expansions are well-suited for efficient echo suppression by spatial filtering. Various new field transformation and new computational performance results are shown in order to illustrate some capabilities of the algorithm.

1. INTRODUCTION

Maxwell's equations have been presented at about 150 years ago [1]. Since that time, the views on electromagnetic fields and the governing equations have been changing and many techniques for the solution of the field equations have been investigated. Nowadays, we concentrate mostly on differential equation based field solutions and on integral representations of the fields due to sources or equivalent sources [2–4]. Integral representations calculate the fields by integrals over the sources together with an analytically known kernel, the Green's function, which is, however, only known for free space or

Received 11 December 2014, Accepted 15 May 2015, Scheduled 18 May 2015
Invited paper for the Commemorative Collection on the 150-Year Anniversary of Maxwell's Equations.
* Corresponding author: Thomas F. Eibert (eibert@tum.de).
The authors are with the Lehrstuhl für Hochfrequenztechnik, TU München, Munich 80290, Germany.

other canonical solution domains. In this paper, we consider integral representations involving Green's functions of free space, which are called field transformations, since the sources are mostly equivalent sources, which are linked to the fields, typically on a Huygens surface. The integral representations are extended by weighting or reaction integrals in order to have access to true field observations by realistic measurement probes, where the influence of the probes is considered by appropriate weighting functions. Moreover, the weighting integral formulation gives access to reaction and reciprocity considerations [2, 5–7] as frequently used in numerical techniques such as the Method of Moments (MoM) [8]. Even though the Green's functions are known analytically, the field transformation and weighting integrals must usually be evaluated numerically. Since the transformations are four to six fold integrals, their numerical solution becomes easily computationally intensive and efficient methods are required to evaluate the field transformations. Another issue with the numerical evaluation of these integrals are the singularities of the involved Green's functions for closely located source and observation points. The accurate evaluation of these singularities is essential for integral equation solutions of radiation and scattering problems, where the radiation integrals must be evaluated in the locations of the equivalent sources in order to enforce the boundary conditions on the radiation or scattering objects [4, 8, 9]. A wide variety of singularity treatments is nowadays available, e.g., see [10, 11], where such techniques are, however, not in the focus of this paper. The focus are field transformations, where weighted field observations are known from measurements or simulations and where equivalent sources reproducing these field observations shall be computed. Since observation and source locations are typically well separated, particular singularity treatment is here not necessary, unless the field transformations are combined with additional constraints such as a null-field condition in order to obtain Love equivalent surface current densities [12–15]. Once the equivalent sources have been determined, they shall be used to compute further field observations of interest, e.g., the far-field of an antenna or a scatterer. Especially antenna field measurements have become more and more important over the past years, since the accurate knowledge of the radiation behavior of antennas is essential to further improve the performance and capabilities of wireless communication and sensor systems. Full knowledge about the radiation or the scattering behavior of an object is obtained by field measurements on a closed surface around the object and by measuring the amplitudes and the phases of the fields. Closed measurement surfaces can be replaced by open ones, if it is clear that the field amplitudes are very low in some region of space or if interest is only in certain radiation directions. Also, phaseless measurements are possible, where the robustness of the transformations is, however, reduced and an increased number of measurement samples should be collected [16–19]. Once appropriate measurements have been taken, field transformations can be utilized to compute the radiation or scattering fields of a Device Under Test (DUT) in any location outside the sources of the DUT and it is even possible to perform DUT diagnostics by evaluating the fields very close to the DUT.

Classical antenna field transformation methods work with modal expansions of the fields, where the advantageous orthogonality of the field modes is utilized for measurements performed on canonical surfaces such as planes, cylinder shells, or spheres. It is also very common to accelerate the computation of the modal expansion coefficients by utilizing the Fast Fourier Transformation (FFT). This leads, however, to the requirement that the measurement samples must be placed regularly, see, e.g., [20] for an overview of modal field transformation techniques. Due to this, the flexibility and the diagnostics capabilities of the conventional antenna field transformation techniques are rather limited and quite often considerably more measurement samples have to be collected than actually required. Another shortcoming of the modal field transformations is that they cannot consider a priori information about the spatial sources distribution of the DUT, except for limiting the number of modes.

Inverse equivalent current or sources reconstruction methods [12, 21–23] work with spatially discretized equivalent sources representations of the DUT. However, the basic equivalent sources methods with spatial integral representation are computationally very demanding, as mentioned before, and their speed-up by fast integral operator evaluation methods is more or less mandatory to transform the measurements of electrically large DUTs. In [24], regularly sampled planar measurements have been transformed with FFT acceleration. The most flexible and useful fast integral operator computation method for this purpose is the Multilevel Fast Multipole Method (MLFMM) [9, 25], which has been adapted in [22, 23] for the solution of inverse equivalent current problems. A single-level FMM has been used in [26]. In contrast to the utilization of MLFMM for the solution of integral equations

related to radiation and scattering problems, the challenges in its use for field transformations and inverse equivalent current problems are the often relatively large separation distance between sources and observation locations, the relatively large spatial separation between different observation locations, and the appropriate treatment of realistic measurement probes.

With the MLFMM formulation for inverse equivalent current problems, it became obvious that the representation with propagating plane waves on the Ewald sphere, opens up completely new possibilities for performing near-field far-field (NFFF) transformations. The key is that the introduced discretized plane wave spectra can directly be utilized as equivalent sources representing the DUT [27, 28]. This resulted in a very efficient algorithm, which we call FIAFTA (Fast Irregular Antenna Field Transformation Algorithm). FIAFTA is able to include the influence of arbitrary measurement probes just by their 3D FF patterns and it offers several possibilities to represent the equivalent sources of the DUT. For instance, in antenna diagnostics, equivalent surface currents on a triangular mesh are useful. The triangular mesh can directly model the enveloping surface of the antenna and the surface current densities can be linked to the radiation fields near the antenna. The plane wave expansion coefficients of a source group according to the MLFMM hierarchy can also be used as unknowns for the inverse problem instead of the expansion coefficients of the surface currents on a triangular mesh. For further reduction of memory consumption and most robust behavior, the plane wave spectrum of a source box can be expanded in orthogonal spherical harmonics whose coefficients are used as unknowns. For these equivalent sources representations, the hierarchical octree structure of the MLFMM helps to localize the sources. Only boxes need to be defined as source boxes, which contain parts of a Huygens surface representing the DUT. A priori knowledge about the device geometry can easily be incorporated into the model for the inverse problem solution for all types of sources.

The ability to position sources arbitrarily within the octree makes it possible to place sources at locations where parasitic echo centers due to scattering objects are assumed during the NF measurement. By spatial filtering of these sources, DUT fields such as the far-field can be computed only from the subset of equivalent sources belonging to the DUT. The influence of the disturbing sources on the measurements is thereby eliminated.

The outline of the paper is as follows. In Section 2, electromagnetic field transformations in form of weighted spatial radiation integrals are introduced and discussed together with uniqueness and complexity considerations. Spectral representations of the field transformation operator are then reviewed in Section 3, where first planar plane wave expansions are discussed, which have a series of unique properties, but whose applicability is restricted to field observations in a plane. Spherical wave expansions are shortly reviewed in order to emphasize its beauty and importance for practical NF antenna measurements. The central part of this section are, however, propagating plane wave expansions on the Ewald sphere. In Section 4, multilevel hierarchical field decompositions are reviewed and discussed, which are the basis of FMM and MLFMM as well as of FIAFTA. These techniques combine the ideas of the before discussed plane wave and spherical harmonics expansions in order to achieve high flexibility and efficieny at the same time. Section 5 concentrates on FIAFTA. Starting from the inverse problem solution concept, the various available sources representations and modelling capabilities are discussed. Finally, Section 6 shows various results obtained by FIAFTA in order to demonstrate its capabilities.

As already mentioned, the paper is mostly a review paper, but the presented transformation and computational performance results are new. Also, many new insights into the algorithms are included. Further capabilities of FIAFTA including the efficient treatment of non-redundant measurements [29, 30], echo suppression techniques by inward and outward looking measurement probes [31], volumetric imaging by hierarchical disaggregation of broadband field observations [32], efficient transformation of phaseless field measurements with first results [18, 19], and the utilization of FIAFTA within non-linear inverse material problem solutions [14, 15, 33] are found in the given references. Extensive error investigations are presented in [34]. Recently, the FIAFTA concept was extended for the NFFF transformation of monostatic radar cross section measurements [35]. A portable antenna measurement system, which can fully benefit from the great transformation flexibility of FIAFTA, has been presented in [36].

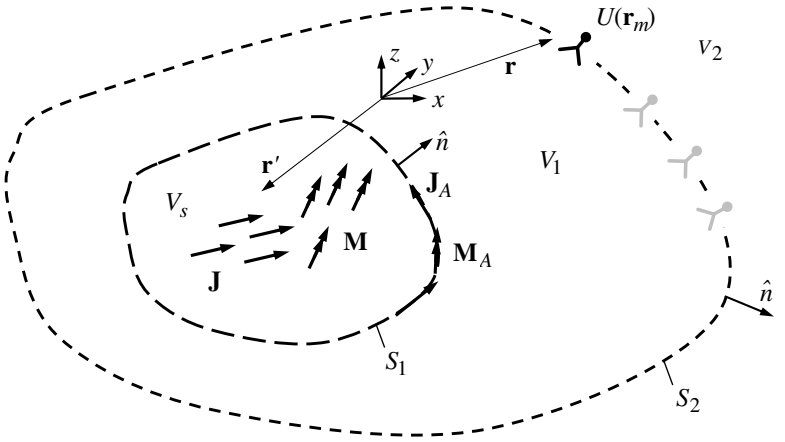

Figure 1. Field transformation configuration: sources $\mathbf{J}$ and $\mathbf{M}$ within V_s bound by the Huygens surface S_1 generate fields which are observed by probe antennas at measurement locations $\mathbf{r}_m$. The radiated fields outside of S_1 can also be generated by equivalent surface current densities $\mathbf{J}_A$ and $\mathbf{M}_A$ on the surface S_1. The fields in V_1 and V_2 can be determined in a unique way from two independent field observations on the surface S_2.

2. FORMULATION OF WEIGHTED FIELD TRANSFORMATIONS

The considered linear field transformations are integrals of the form

$$U(\mathbf{r}_m) = \iiint\limits_{V_w} \mathbf{w}(\mathbf{r}-\mathbf{r}_m) \cdot \iiint\limits_{V_s} \left[\bar{\mathbf{G}}_J^E(\mathbf{r},\mathbf{r}') \cdot \mathbf{J}(\mathbf{r}') + \bar{\mathbf{G}}_M^E(\mathbf{r},\mathbf{r}') \cdot \mathbf{M}(\mathbf{r}')\right] dv' dv\,, \tag{1}$$

for time harmonic fields and sources with a suppressed time factor $\mathrm{e}^{j\omega t}$ dependent on the angular frequency ω. The transformation configuration is illustrated in Fig. 1 and as usual, $\mathbf{r}'$ denotes source locations, $\mathbf{r}$ observation locations, and $\mathbf{w}$ is a vector weighting function, which produces a field observation in form of the voltage U[†] at the location $\mathbf{r}_m$. $\mathbf{J}$ and $\mathbf{M}$ are the electric and magnetic source current densities and $\bar{\mathbf{G}}_J^E$ and $\bar{\mathbf{G}}_M^E$ are the corresponding dyadic Green's functions, respectively, which are known analytically, as, e.g., for free space in the form of

$$\bar{\mathbf{G}}_J^E(\mathbf{r},\mathbf{r}') = -j\frac{\omega\mu}{4\pi}\left(\bar{\mathbf{I}} + \frac{1}{k^2}\nabla\nabla\right)\frac{\mathrm{e}^{-jk|\mathbf{r}-\mathbf{r}'|}}{|\mathbf{r}-\mathbf{r}'|}, \quad \bar{\mathbf{G}}_M^E(\mathbf{r},\mathbf{r}') = -\frac{1}{4\pi}\nabla\times\bar{\mathbf{I}}\,\frac{\mathrm{e}^{-jk|\mathbf{r}-\mathbf{r}'|}}{|\mathbf{r}-\mathbf{r}'|}\,. \tag{2}$$

k is here the wavenumber of free space, μ the permeability of free space, and $\bar{\mathbf{I}}$ the unit dyad.

In many cases, it is useful to work with surface current densities $\mathbf{J}_A$ and $\mathbf{M}_A$ as well as with surface weighting functions $\mathbf{w}_A$ defined in locations $\mathbf{r}_A$ on surfaces, which are linked to the corresponding volume densities via

$$\mathbf{J}(\mathbf{r}) = \mathbf{J}_A(\mathbf{r})\,\delta(\mathbf{r}-\mathbf{r}_A)\,, \quad \mathbf{M}(\mathbf{r}) = \mathbf{M}_A(\mathbf{r})\,\delta(\mathbf{r}-\mathbf{r}_A)\,, \quad \mathbf{w}(\mathbf{r}) = \mathbf{w}_A(\mathbf{r})\,\delta(\mathbf{r}-\mathbf{r}_A)\,. \tag{3}$$

Based on Huygens principle, the surface current densities can be related to the tangential fields by

$$\mathbf{J}_A(\mathbf{r}) = \hat{n}\times\mathbf{H}(\mathbf{r})\,, \quad \mathbf{M}_A(\mathbf{r}) = -\hat{n}\times\mathbf{E}(\mathbf{r})\,, \tag{4}$$

where $\hat{n}$ is the unit normal vector on an appropriate Huygens surface. If the equivalent surface currents or the tangential fields are known on closed Huygens surfaces or if open surfaces can be closed by surface extensions with vanishing tangential fields, Huygens and equivalence principles can be used for the derivation of uniqueness statements of the transformed fields or observables according to (1). Important for this to be valid is that the field transformations are only performed in source free regions. For the case in Fig. 1, it is, e.g., required that the relevant primary sources $\mathbf{J}$ and $\mathbf{M}$ are confined to

[†] U can be an open-circuit voltage or the voltage at a certain load impedance.

the region V_s[‡]. With knowledge of the equivalent surface currents on one of the surfaces S_1 or S_2 in Fig. 1, the electromagnetic fields are uniquely defined anywhere in space (in V_1 and in V_2) except for the volume V_s with the original sources. In case of radiation problems, the primary sources are contained in V_s, whereas for scattering problems, it is assumed that the sources of the scattered fields are confined to V_s and that these sources are induced by an incident field. (1) relates then to the scattered fields.

In NF measurements, the complex fields (amplitude and phase) are usually measured on the surface S_2 (utilizing appropriate measurement probes) and equivalent sources within V_s or on S_1 are determined from these measurements in order to reproduce the measurements. Then, the found equivalent sources are used to compute the far-fields or near-fields anywhere in V_1 and V_2. The determination of the equivalent sources within V_s or on S_1 is a linear inverse problem solution with a forward operator in the form of (1). The inverse problem solution is in particular necessary in order to remove the influence of the measurement probe antennas represented by the weighting function $\mathbf{w}$ in (1).

For the transformation of simulated near-fields, an inverse problem solution is usually not required, since the fields are directly accessible without a measurement probe. Consequently, any observation field in V_1 or V_2 can be computed directly from the also known equivalent sources $\mathbf{J}_A$ and $\mathbf{M}_A$ on S_1 by evaluating (1) in the form of a forward operator.

According to the uniqueness theorem, it is known that the knowledge of one type of tangential surface fields (electric or magnetic) is sufficient to uniquely define the electromagnetic fields in the whole volume enclosed by the surface as long as no resonances occur. In field transformations as, e.g., for measurements of radiation or scattering fields, it is commonly assumed that resonances cannot occur and, therefore, only one type of measurement (with a certain measurement probe) is usually performed[§]. Also, it is noted that one type of equivalent surface currents, e.g., on S_1 in Fig. 1, is sufficient to reproduce any field in V_1 or V_2, even though the surface current densities and the corresponding fields do no longer fulfill (4) in this case. If both types of surface current densities are present during the inverse solution process, they are not uniquely defined anymore and they can contain non-radiating currents. These non-radiating currents are not harmful to the field transformation in most cases, but they can be suppressed by further constraint equations forcing the fields inside V_s to be zero, if required. In this case, $\mathbf{J}_A$ and $\mathbf{M}_A$ are unique and fulfill (4) [12, 14, 15].

In real field measurements, the weighting function $\mathbf{w}$ represents the measurement probe and one may ask what the physical meaning of $\mathbf{w}$ is. The question can be resolved by looking at different equivalent reciprocity interaction integral representations for the probe antenna. Fig. 2(a) illustrates a possible measurement probe, where U is the receive voltage for a given incident field and I is the feed current of the probe antenna in transmit mode, which is impressed in the terminal region. Fig. 2(b) shows an equivalent representation of the same antenna, where the antenna structure has been replaced by an equivalent electric current distribution impressed within the probe volume V_w. By invoking the equivalence principle [2], it can be shown that both configurations radiate the same fields in transmit mode[‖]. Together with the reciprocity theorem [2], it can then be shown that

$$U(\mathbf{r}_m)I(\mathbf{r}_m) = \iiint\limits_{V_w} \mathbf{E}(\mathbf{r}) \cdot I(\mathbf{r}_m)\mathbf{w}(\mathbf{r}-\mathbf{r}_m)dv \quad \longrightarrow \quad U(\mathbf{r}_m) = \iiint\limits_{V_w} \mathbf{E}(\mathbf{r}) \cdot \mathbf{w}\left(\mathbf{r}-\mathbf{r}_m\right) dv. \tag{5}$$

Consequently, the probe weighting function $\mathbf{w}$ can be any equivalent current density impressed in free space representing the probe radiation in transmit mode for a feed current of 1 A at the terminals of the antenna.

In any numerical evaluation of (1) or of the corresponding inverse problem, the sources are discretized by a finite set of basis functions and a finite number of observations are considered. Due to the global nature of the forward operator (1), its direct evaluation will cause a numerical complexity of $\mathcal{O}(MN)$, if M is the number of measurement samples and N the number of basis functions representing the sources. Since this quadratic complexity (assuming $M = N$) will quickly lead to unacceptable computation times for large problems, it is mandatory that efficient numerical methods are constructed for the representation of (1) or its inverse.

[‡] Please note that these primary sources can be due to the DUT, but also due to undesired echo contributions.

[§] As discussed in [31], measurements with different types of probes, e.g., inward and outward looking, can be used to distinguish between sources within and outside of the measurement surface (S_2 in Fig. 1)

[‖] For this, it is assumed that mutual interactions involving the probe antenna are negligible.

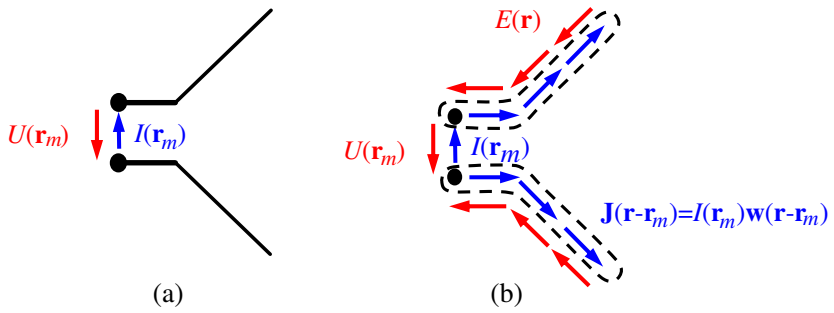

Figure 2. (a) Probe antenna with transmit feed current and receive voltage. (b) Equivalent probe model with removed antenna structure and impressed transmit electric current density in free space.

3. SPECTRAL REPRESENTATIONS OF THE FIELD TRANSFORMATIONS

The key for an efficient evaluation of the forward operator (1) is to eliminate its inherent redundancy. This redundancy is due to the fact that the waves generated by sources in a certain volume can be represented by a limited number of degrees of freedom dependent on the required accuracy. To achieve a redundancy reduction, the waves radiated by the sources are expanded into a set of linearly independent wave objects, which are often solutions of Maxwell's equations and which are orthogonal with respect to each other. Similarly, the weighting functions $\mathbf{w}$ in (1) are only sensitive to a limited number of degrees of freedom of the incident wave field. This fact can be used for a further redundancy reduction by expanding the receive fields at the location of a weighting function into appropriate wave field objects. Since the wave field objects for the expansion of radiated fields are usually outgoing waves and the optimal expansion fields around the weighting functions or receivers are incident waves, translation operators may additionally be needed to convert the outgoing wave expansions into incident wave expansions. The efficiency of these translations is also very important for the overall efficiency, which can be achieved for the evaluation of (1) or for the corresponding inverse problem solution.

3.1. Planar Plane Wave Expansion

One of the simplest wave expansions is found by expanding the fields or equivalently the pertinent Green's functions in (2) in a plane of infinite extent into plane waves. Formally, the Sommerfeld identity [2]

$$\frac{1}{4\pi}\frac{\mathrm{e}^{-jk|\mathbf{r}-\mathbf{r}'|}}{|\mathbf{r}-\mathbf{r}'|} = \int_{-\infty}^{+\infty}\int \frac{\mathrm{e}^{-jk_z|z-z'|}}{k_z}\mathrm{e}^{-jk_x(x-x')}\mathrm{e}^{-jk_y(y-y')}dk_x dk_y \tag{6}$$

with $k_z = \sqrt{k^2 - k_x^2 - k_y^2}$ can be used to achieve this, where the field expansion is here performed in a plane $z = const.$. Assuming only electric current sources and that all sources are below the expansion plane with all observation locations above the expansion plane, (1) together with the Sommerfeld identity (6) can be written in form of

$$U\left(\mathbf{r}_m\right) = -j\omega\mu \int_{-\infty}^{+\infty}\int \left[\check{\mathbf{w}}(k_x,k_y)\mathrm{e}^{-jk_z(z_m-z_s')}\cdot\check{\mathbf{J}}(k_x,k_y)\right]\mathrm{e}^{jk_x x_m}\mathrm{e}^{jk_y y_m}dk_x dk_y \tag{7}$$

with

$$\check{\mathbf{J}}(k_x,k_y) = \iiint_{V_s}\left[\frac{1}{k_z}\left(\bar{\mathbf{I}}+\frac{1}{k^2}\nabla'\nabla'\right)\mathrm{e}^{jk_x x'}\mathrm{e}^{jk_y y'}\mathrm{e}^{jk_z(z'-z_s')}\right]\cdot\mathbf{J}\left(\mathbf{r}'\right)\,dv' \tag{8}$$

and

$$\check{\mathbf{w}}(k_x,k_y) = \iiint_{V_w}\mathbf{w}\left(\mathbf{r}-\mathbf{r}_m\right)\mathrm{e}^{-jk_x(x-x_m)}\mathrm{e}^{-jk_y(y-y_m)}\mathrm{e}^{-jk_z(z-z_m)}\,dv. \tag{9}$$

It is obvious that $\check{\mathbf{J}}$ and $\check{\mathbf{w}}$ are the Fourier or inverse Fourier transforms of the source currents and the weighting or receiving function, respectively, which are related to the corresponding FF patterns as known from antenna theory. z_s' is here chosen as a reference z-location for the sources Fourier transform. The weighting function Fourier transform is defined with respect to a local coordinate system with its origin located in the measurement location $\mathbf{r}_m$ and is, therefore, independent from $\mathbf{r}_m$. Writing the received signal as a Fourier integral

$$U\left(\mathbf{r}_m\right) = \iint_{-\infty}^{+\infty} \check{U}(k_x, k_y) \mathrm{e}^{jk_x x_m} \mathrm{e}^{jk_y y_m} dk_x dk_y \tag{10}$$

and by utilizing the orthogonality of the exponentials with respect to k_x and k_y, we obtain

$$\check{U}(k_x, k_y) = \check{\mathbf{w}}(k_x, k_y) \mathrm{e}^{-jk_z(z_m - z_s')} \cdot \check{\mathbf{J}}(k_x, k_y), \tag{11}$$

where the plane wave expansion of the received signal is usually obtained by regularly sampling the receive field with a given measurement probe with fixed orientation within a measurement plane. In this case, the plane wave expansion in (10) can be efficiently obtained by FFT. In planar antenna measurements, the receive signals $U(\mathbf{r}_m)$ are measured with a measurement probe, $\check{U}$ is computed by FFT and the algebraic Equation (11) is inverted to obtain $\check{\mathbf{J}}$. Usually, two linearly independent (possibly orthogonal) measurement probes are used in order to find the relevant vector components of $\check{\mathbf{J}}$. Once $\check{\mathbf{J}}$ has been determined, the far-field is found from [20]

$$\mathbf{E}^{FF}(\vartheta, \varphi) = k\omega\mu \cos(\vartheta) \frac{\mathrm{e}^{-jkr}}{2\pi r} \check{\mathbf{J}}\left(k \sin(\vartheta)\cos(\varphi), k \sin(\vartheta)\sin(\varphi)\right) . \tag{12}$$

An important advantage of the planar plane wave expansion is that radiated wave objects are identical to incident wave objects, i.e., both are just plane waves. As seen in (7), only a phase shift is needed to translate the radiated waves into incident waves at the observation locations. Since every radiated wave is directly translated into just one incident wave, this translation operator is called diagonal. Writing it in matrix form, it is different from zero only on the main diagonal.

An interesting property of the planar plane wave expansion is the strict separation of propagating and evanescent waves with respect to the expansion plane. Since the evanescent waves do not transport energy from the sources to the observation probes in antenna measurements[¶], they can be completely omitted in antenna field transformations. This separation of evanescent and propagating waves can also be considered as a reason for the fact that supergain effects of antennas are usually only observed in endfire and frontfire directions, but not at broadside.

Practical NF measurements and numerical evaluations of the field transformations require a discretization of the plane wave spectra, where it is commonly accepted that sample spacings of half a wavelength λ are required in planar NF measurements [20]. This is, however, only the case, if FFT based field transformations are utilized, which are not able to consider any a priori knowledge about the DUT. If the knowledge about the shape of the DUT is considered and more flexible field transformation approaches are employed, reduced sampling rates can be achieved for many configurations [29, 30, 37–39].

More information on planar NF measurements and the corresponding FFT based NFFF transformations can, e.g., be found in [20, 40].

3.2. Spherical Wave Expansion

Spherical wave expansions are based on electromagnetic eigenmodes in spherical coordinate systems. Similar to (6), the scalar Green's function can be expanded in form of [2]

$$\frac{1}{4\pi} \frac{\mathrm{e}^{-jk|\mathbf{r}-\mathbf{r}'|}}{|\mathbf{r}-\mathbf{r}'|} = -jk \sum_{n=1}^{\infty} \sum_{m=-n}^{n} \mathrm{j}_n(kr') \mathrm{h}_n^{(2)}(kr) \mathrm{Y}_{nm}^*(\vartheta', \varphi') \mathrm{Y}_{nm}(\vartheta, \varphi) \tag{13}$$

where the radiating wave expansion with respect to $\mathbf{r}$ consists now of outgoing spherical waves containing the spherical Hankel functions $\mathrm{h}_n^{(2)}$ of 2nd kind and order n together with the spherical harmonics Y_{nm}.

[¶] This is true as long as mutual coupling between the sources and the probes is neglected, what is a common assumption in antenna and scattering measurements.

The source expansion consists of standing waves with respect to the radial direction involving the spherical Bessel functions j_n of order n together with the conjugate complex of Y_{nm} (indicated by the *), i.e., radiating and incident wave field objects are now different. This expansion can again be plugged into (1) in order to obtain a spectral representation of the field transformation. If source current densities are given and their fields shall be evaluated, it is necessary to first compute the integral over $\mathbf{r}'$ in order to obtain the multipole expansion coefficients of the radiating spherical waves. However, in the inverse problem case, where field observations are given, it is usually possible to avoid the $\mathbf{r}'$ integrations and the multipole coefficients of the outgoing waves are directly determined in the inverse solution process. The FF pattern of the DUT can be directly obtained from these multipole coefficients by evaluating the outgoing waves under FF conditions.

In order to facilitate the evaluation of the transformation equation, the weighting function $\mathbf{w}$ representing the measurement probe, is usually first represented with a spherical expansion of radiating or receiving waves in a local probe coordinate system and this expansion is then translated into weighting coefficients for the radiating modes in the DUT coordinate system [20, 41]. In general, such multipole translations are full operators. However, under the assumption of probes with first order azimuthal modes only, these translations can be performed very efficiently. Together with regular sampling in ϑ and φ on spherical measurement surfaces, the resulting spectral operator can be evaluated very efficiently in forward as well as in inverse direction by utilizing FFTs [20, 41]. The corresponding extremely efficient algorithms are nowadays the standard in spherical NFFF transformations. For higher order azimuthal probes, also a variety of field transformation algorithms have been investigated, which are, however, less efficient [42, 43].

An interesting property of the spherical modes is that they do not allow the separation of evanescent and purely energy propagating modes. Actually every single outgoing mode becomes strongly evanescent if the radius r is just chosen small enough. Usually, the sampling requirements of the spherical modes are derived based on this observation. Dependent on the desired accuracy, modes which are strongly evanescent in the source region are assumed to decay far enough until they become predominantly propagating [9].

An important advancement to mention is the combination of spherical mode expansions with complex source or Gaussian beams, which allow directive wave field representations [44].

3.3. Propagating Plane Wave Expansion on the Ewald Sphere

An alternative plane wave based expansion of the scalar Green's function is given by [9]

$$\frac{\mathrm{e}^{-jk|\mathbf{r}-\mathbf{r}'|}}{|\mathbf{r}-\mathbf{r}'|} = \oiint \mathrm{e}^{-j\mathbf{k}\cdot(\mathbf{r}-\mathbf{r}_m)}\mathrm{e}^{j\mathbf{k}\cdot(\mathbf{r}'-\mathbf{r}'_s)}\, T_\infty\left(\hat{k}, \mathbf{r}_m-\mathbf{r}'_s\right)\, d\hat{k}^2 \tag{14}$$

valid for arbitrary vectors with $|\mathbf{r}_m-\mathbf{r}'_s| > |\mathbf{r}-\mathbf{r}_m-\mathbf{r}'+\mathbf{r}'_s|$ with the diagonal translation operator

$$T_\infty(\hat{k}, \mathbf{X}) = \frac{jk}{4\pi}\sum_{l=0}^{\infty}(-j)^l(2l+1)\,\mathrm{h}_l^{(2)}(k|\mathbf{X}|)\,\mathrm{P}_l\left(\hat{k}\cdot\hat{X}\right) \tag{15}$$

as known from FMM. P_l is the Legendre polynomial of order l. $\mathbf{r}_m$ can here be chosen as the measurement location or as the reference point of a cluster of measurement probes and $\mathbf{r}'_s$ can be chosen as a reference point of the sources or a cluster of sources. As obvious from the given condition for the location vectors, the volume containing the sources is not allowed to overlap here with the volume containing the observation locations. Plugging this expansion in (1), we obtain

$$U\left(\mathbf{r}_m\right) = \frac{-j}{4\pi}\oiint\left[\tilde{\mathbf{w}}(-\mathbf{k})\cdot T_\infty(\hat{k}, \mathbf{r}_m-\mathbf{r}'_s)\,\left(\tilde{\mathbf{J}}(\mathbf{k})+\tilde{\mathbf{M}}(\mathbf{k})\right)\right] d\hat{k}^2 \tag{16}$$

with

$$\tilde{\mathbf{J}}(\mathbf{k}) = -j\frac{\omega\mu}{4\pi}\iiint_{V_s}\left(\bar{\mathbf{I}}-\hat{k}\hat{k}\right)\cdot\mathbf{J}\left(\mathbf{r}'\right)\mathrm{e}^{j\mathbf{k}\cdot(\mathbf{r}'-\mathbf{r}'_s)}dv', \tag{17}$$

$$\tilde{\mathbf{M}}(\mathbf{k}) = j\frac{k}{4\pi}\iiint\limits_{V_s}\left(\hat{k}\times\mathbf{M}\left(\mathbf{r}'\right)\right)\mathrm{e}^{j\mathbf{k}\cdot(\mathbf{r}'-\mathbf{r}'_s)}dv', \tag{18}$$

and

$$\tilde{\mathbf{w}}(\mathbf{k}) = \iiint\limits_{V_w}\mathbf{w}\left(\mathbf{r}-\mathbf{r}_m\right)\mathrm{e}^{j\mathbf{k}\cdot(\mathbf{r}-\mathbf{r}_m)}\,dv. \tag{19}$$

As already noted, we have here again a diagonal translation operator for plane waves, where the dependence on the measurement location is, however, relatively complicated. Therefore, an orthogonal expansion with respect to measurement locations $\mathbf{r}_m$ varying on a certain surface shape is not possible with this representation. The strength of this formulation is its great flexibility and independence from particular measurement surface shapes. The field transformation equation can be evaluated in any direction as long as the source and observation volumes do not overlap and it captures evanescent field effects with a purely propagating plane wave representation. In antenna field transformations, it has been observed that this transformation can directly work with a discretized representation of $\tilde{\mathbf{J}}$, i.e., of the DUT radiation pattern, without resembling to the spatial source currents [28]. The transformation can, however, also be used to speed up the inverse computation of spatial equivalent currents representing a DUT or a scattering object [22, 23] or for just evaluating the fields radiated from known sources. Most advantageous is this propagating plane wave based field transformation within a hierarchical scheme for the representation of the sources and the observations as discussed in the next Section 4.

Quite interesting to investigate is the behavior of (16) for large translation distances $|\mathbf{r}_m - \mathbf{r}'_s|$. In accordance with what can be expected from the common FF approximations, it turns out that the FMM translation operator can be replaced by [45]

$$T^{FF}(\mathbf{r}_{tr}) = \frac{\mathrm{e}^{-jk|\mathbf{r}_{tr}|}}{|\mathbf{r}_{tr}|}\delta\left(\hat{k}-\hat{r}_{tr}\right) \quad \text{with} \quad \mathbf{r}_{tr} = \mathbf{r}_m - \mathbf{r}'_s \tag{20}$$

for large enough translation distances. This means that only one locally plane wave representing a spherical wave front is incident in V_w. In order to bridge the gap between the classical translation operator (15) and its FF representation (20), windowed translation operators have been proposed as an approximation of (15) for relatively large propagation distances resulting in ray-propagation fast multipole algorithms [46]. More recently, the concept of Gaussian beams has been introduced by T. Hansen in [47], which provides a rigorous directive representation of the FMM translation operator according to

$$T^{GB}_{\infty}\left(\hat{k},\mathbf{X}\right) = \frac{jk}{4\pi}\sum_{l=0}^{\infty}(-j)^l(2l+1)\,\mathrm{h}^{(2)}_l\left(k\left(|\mathbf{X}|-j\Delta\right)\right)\mathrm{P}_l\left(\hat{k}\cdot\hat{X}\right) \tag{21}$$

where a complex translation distance with an imaginary part $-\Delta$ ($\Delta > 0$) is used. An observation, which can be concluded from the existence of different exact translation operators, is that many incident wave spectra composed of propagating plane waves on the Ewald sphere can produce the correct incident field in the observation volume.

4. MULTILEVEL HIERARCHICAL SOURCES AND FIELD REPRESENTATIONS

A limitation of the discussed spectral representations of the field transformation integral (1) is given by the fact that the source volumes and the observation volumes must not overlap in order to ensure convergence of the spectral series or integral representations. In the planar plane wave representation, the sources and the observation locations must be on opposite sides of an infinite plane, what is usually only given for planar NF measurements. In the spherical mode expansion and in the Ewald sphere based plane wave expansion, the minimum spheres around the sources and around the considered weighting functions at the observation locations must not overlap. These restrictions can be very severe for practical configurations. However, the restrictions can be overcome by hierarchical evaluations of the field transformations. The idea is to first organize the sources and the observation weighting functions into localized clusters. Then, the field transformations are performed for well separated

clusters and observers until the interactions between all source clusters and all observation clusters have been captured. If the cluster sizes are fixed at a relatively small size, the computational complexity will remain at $\mathcal{O}(MN)$, as discussed in Section 2. However, with a multilevel hierarchical clustering scheme of the sources and the observers a numerical complexity of $\mathcal{O}(M\log(M)+N\log(N))$ can be achieved for the evaluation of all the interactions. The hierarchical clustering is usually achieved by an octree based spatial partitioning [9]. First, all sources and/or observers are enclosed in a large cube on the coarsest level. Next, this cube is subdivided into eight equal sized sub-cubes on the first finer level. Then, every cube on this finer level is again subdivided and so on, until the cubes are so small that all relevant field interactions can be accurately computed. If sources and observers are so close that their interactions cannot be computed by the utilized spectral representation, the spatial field interaction integral (1) can be utilized for the computation of these interactions. If it is desired to work with a particular cube size on the finest level, it is advantageous to build the octree from the finest level to the coarser levels. In most cases, the sources and the observers are organized within the same octree, but sometimes separate octrees for the sources and the observers can be of benefit [32, 35].

The spectral field transformations basically consist of three steps: 1.) The computation of the spectral sources and observer representations on the source and the testing levels, respectively. 2.) The translation of the spectral representations from the source boxes to the observation boxes. This includes aggregation of the sources spectral representations from finer to coarser levels, so that the translations can be performed on the most appropriate levels. At the receiving side, the received spectra are disaggregated down to the testing or observation level. 3.) The evaluation of the spectral series or integrals on the testing level.

For the efficiency of a hierarchical multilevel scheme, it is essential that the aggregations and disaggregations of the spectral representations among different levels can be evaluated with low computational complexity. Since aggregations and disaggregations are usually full operators for the spherical multipole based spectral representations, these expansions are not very convenient for high-frequency applications [9]. In the spectral plane wave based representations, the aggregations and disaggregations require interpolations and phase shifts, which can be performed very efficiently with a complexity of $\mathcal{O}(N\log(N))$ for local interpolation or $\mathcal{O}(N\log^2(N))$ for global interpolation (similarly for M) [9]. Hierarchical multilevel schemes utilizing Ewald sphere based plane wave spectral representations have become famous in the so-called Multilevel Fast Multipole Method (MLFMM) or Multilevel Fast Multipole Algorithm (MLFMA) for the solution of integral equations [9]. Such integral equation

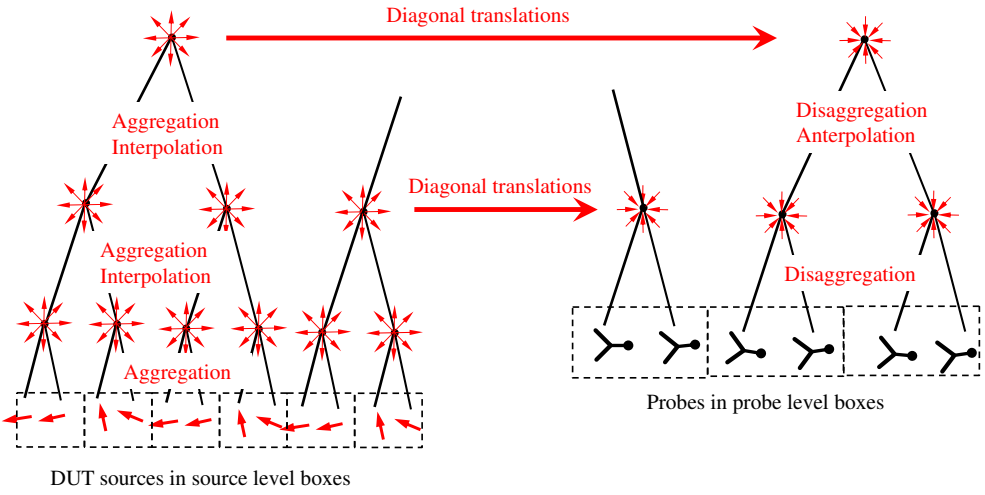

Figure 3. Hierarchical field transformation: Spectral sources representations are first computed with respect to the box centers of the source level. Next, the spectral sources are interpolated and aggregated to coarser levels. Diagonal field translations are performed on the most appropriate level. The plane waves in the receiver boxes are disaggregated and anterpolated until the interactions with the measurement probes are computed on the testing level, which can be different from the source level.

problems are characterized by the fact that sources and observation weighting functions are more or less identical and populate the same volume. Therefore, relatively many near-interactions have to be computed. In [48], also field interactions from known sources to observation locations have been computed based on MLFMM. In [22, 23], inverse equivalent current problems have been solved by utilizing hierarchical multilevel representations and in [27, 28], the NFFF transformations have been directly performed with the spectral plane wave representation of the DUT radiation pattern. In Fig. 3, the hierarchical multilevel scheme is illustrated for the computation of the received probe fields due to equivalent current sources representing a DUT.

A planar plane wave expansion based multilevel algorithm has been presented in [49] for the solution of a planar integral equation formulation.

5. THE FAST IRREGULAR ANTENNA FIELD TRANSFORMATION ALGORITHM

FIAFTA is basically an algorithm for the computation of equivalent surface current densities $\mathbf{J}_A$ and $\mathbf{M}_A$ on a surface S_1 as illustrated in Fig. 1 due to field observations in arbitrary locations obtained with arbitrary measurement probes with arbitrary orientation. Usually, the measurement locations lie on a closed or open (e.g., for planar) surface S_2 around a DUT, which is assumed to radiate. Alternatively, a scattering problem can be considered, where an incident wave exists, e.g., a plane wave or an illuminating antenna in the near-field. In order to formulate the linear inverse problem, the M field observations are collected in the solution column vector $\mathbf{b}$ and the sources are discretized with a set of N known basis functions with N unknown coefficients collected in the column vector $\mathbf{x}$. Thus, the linear transformation operator Equation (1) can be written in the form of a linear equation system

$$\bar{\mathbf{C}}\,\mathbf{x} = \mathbf{b}, \tag{22}$$

where the M by N matrix $\bar{\mathbf{C}}$ contains the field interactions between the source basis functions and the weighting functions representing the measurement probes. Since this equation system is usually under or overdetermined and may contain noise and interference due to imperfect measurements, we solve the corresponding normal equation system

$$\bar{\mathbf{C}}^{ad}\,\bar{\mathbf{C}}\,\mathbf{x} = \bar{\mathbf{C}}^{ad}\mathbf{b}, \tag{23}$$

which gives a least mean square solution for $\mathbf{x}$ [50]. $\bar{\mathbf{C}}^{ad}$ is here the adjoint (transpose conjugate complex) of $\bar{\mathbf{C}}$. The normal equation system is solved by the iterative Generalized Minimal Residual (GMRES) equation solver [51], which has built-in regularization properties and can be stopped before noise or interference start to strongly influence the solution quality. Important is also that an iterative solver does not need the explicit inversion of the forward operator, but only the repeated evaluation of the matrix-vector products involving $\bar{\mathbf{C}}$ and $\bar{\mathbf{C}}^{ad}$ for the solution of the inverse problem.

5.1. Spatial Domain Discretization of Equivalent Surface Current Densities

In FIAFTA, we work with surface current densities according to (3) and (4), which are discretized on triangular meshes according to

$$\mathbf{J}_A(\mathbf{r}) = \sum_p J_p \boldsymbol{\beta}_p(\mathbf{r}) \quad \text{and} \quad \mathbf{M}_A(\mathbf{r}) = \sum_q M_q \boldsymbol{\beta}_q(\mathbf{r}) \;, \tag{24}$$

where $\boldsymbol{\beta}_p$ and $\boldsymbol{\beta}_q$ are divergence conforming vector basis functions. Mostly, we work with the well known Rao-Wilton-Glisson (RWG) basis functions, but higher-order basis functions can also be used [23]. The expansion coefficients J_p and M_q are the unknowns of the inverse problem.

In an initial step of the inverse problem solution, the vector basis functions are grouped in the boxes on an appropriate level of an octree as discussed in Section 4 and the plane wave spectra on the Ewald sphere according to (17) and (18) are computed with respect to the box centers. The probe spectral representation according to (19) can also be precomputed, if the spatial probe weighting function $\mathbf{w}$ is known as, e.g., in the case of a Hertzian dipole probe or an open-ended waveguide probe. For realistic measurement probes, however, the FF radiation pattern is usually known from measurements or external simulations and it can directly be used as $\tilde{\mathbf{w}}$.

In the iterative solution of the inverse problem in (23), the matrix operators $\bar{\mathbf{C}}$ and $\bar{\mathbf{C}}^{ad}$ are usually computed on the fly according to (16) and by utilizing the hierarchical multilevel principles in Section 4 together with the pre-computed spectral representations of $\boldsymbol{\beta}_p$ and $\boldsymbol{\beta}_q$ as well as of all $\tilde{\mathbf{w}}$ for the various testing locations $\mathbf{r}_m$. For very small translation distances from the sources to the observation weighting functions, the field interactions can also be computed by direct spatial integration according to (1).

Once the inverse problem solution has been obtained, the J_p and M_q are known and can be used to compute the true $\tilde{\mathbf{J}}$ and $\tilde{\mathbf{M}}$ in (17) and (18) with respect to the corresponding octree box centers and the total far-field of the DUT is efficiently obtained by aggregating and interpolating all the source box far-fields to coarser levels of the octree until the level with only one box representing the total pattern has been reached. Unknown radiation or scattering fields in NF locations can be obtained by evaluating (1) or (16) with Dirac delta weighting functions at the desired locations.

Valuable diagnostic information about the DUT can be obtained by visualization of the surface current densities on the underlying triangular meshes and it is also possible to perform spatial filtering of the surface current densities before the near-fields or far-fields are finally evaluated. In particular, if disturbing scattering objects influence the field measurements, they can also be modelled by equivalent current densities during the inverse problem solution and later discarded within the FF or NF computations. Such spatial filtering of equivalent sources can achieve a considerable suppression of echo contributions, in particular if the location of the echo sources is known. A typical NF transformation scenario with equivalent surface current densities placed in the source boxes of an octree structure is illustrated in Fig. 4(a).

As discussed in [23] and in the initial problem statement in this paper, working with electric and magnetic surface current densities on a Huygens surface as, e.g., S_1 in Fig. 1 leads to a redundant source representation. By scaling the electric and magnetic surface current densities appropriately, the resulting solution for the equivalent sources can be influenced while the far-fields and near-fields computed from these sources remain the same as long as the observation point is located, e.g., outside of V_s in Fig. 1. Alternatively, the fields in V_S can be forced to zero by additional constraint equations in order to obtain the so-called Love current densities according to (4) [12, 14, 15].

5.2. Direct Discretization of the Plane Wave Spectra of the Source Boxes

Instead of performing the transition from the spatial into the spectral domain according to (17) and (18), the sum of the spectra $\tilde{\mathbf{J}}$ and $\tilde{\mathbf{M}}$ can be sampled directly dependent on $\hat{k}(\vartheta, \varphi)$. The number of the corresponding plane wave samples depends on the size of the chosen source boxes, determining the maximum spectral content of the generated fields. In order to accurately evaluate the spectral integral in (16), the translation operator must also be sampled appropriately. For this purpose, a Gauss-Legendre quadrature rule with $N_{pw} = 2(L+1)^2$ plane wave samples on the Ewald sphere is typically utilized [25]. Choosing the sampling rate according to the quadrature rule leads to an oversampling of the plane wave spectra of the source boxes. This is of course disadvantageous for the memory consumption and the well-posedness of the inverse problem, but beneficial for the accuracy of the interpolation process, if a local Lagrange interpolation method is employed in the aggregation step of the algorithm [9]. Such an oversampling makes it necessary to carefully low-pass filter the plane wave spectra in order to limit their bandwidth according to the size of the source boxes. As an alternative, global interpolation by FFT can also be used within the aggregation and disaggregation procedures. Since global interpolation is exact for band limited signals, oversampling can be omitted in this case. However, the equidistant plane wave samples on the sphere must be considered as 2π periodic in ϑ, too, and the numerical integration involving the metric coefficient $|\sin(\vartheta)|$ must be appropriately handled in the numerical quadrature over the sphere based on equidistant sampling. Details about the corresponding algorithms for radiation and scattering integral equation solutions can be found in [52–54].

5.3. Spherical Harmonics Expansion of the Plane Wave Spectra of the Source Boxes

The plane wave spectra of the source boxes mentioned before can be expanded in spherical harmonics according to[+] [25]

$$\tilde{\mathbf{J}}\left(\mathbf{k}(\vartheta,\varphi)\right)+\tilde{\mathbf{M}}\left(\mathbf{k}(\vartheta,\varphi)\right)=\mathbf{T}\left(\mathbf{k}(\vartheta,\varphi)\right)\sum_{m=0}^{M_L}\sum_{n=-m}^{m}\mathbf{f}_{mn}\mathrm{Y}_{mn}\left(\mathbf{k}(\vartheta,\varphi)\right) \tag{25}$$

where $\mathbf{f}_{mn}$ are expansion coefficients in Cartesian components and $\mathrm{Y}_{mn}\left(\mathbf{k}(\vartheta,\varphi)\right)$ are scalar spherical harmonics of degree m and order n [9, 25]. The Cartesian vector components are transformed into the required spherical ϑ- and φ-components by the matrix operator $\mathbf{T}$. The necessary maximum degree M for the representation of the plane wave spectra of a source box again must be chosen according to the size of the box. Usually, a number of $M_L = L/2 - 1$ spherical harmonics is sufficient, where L is the chosen truncation order in (16) and with the assumption of source and receive boxes of equal size. As a result, $N_{sph} = 3(L/2-1)$ spherical harmonics for each source box are needed. The advantage of the expansion in spherical harmonics is that the number of unknowns of the inverse problem can be kept minimal. Also, the spherical harmonics form an orthogonal basis which is very well suited for a robust representation of the radiation characteristics of the source boxes. Furthermore, the direct evaluation of the spherical harmonics allows for an exact low-pass filtered transition to the plane wave representation on the source level of the octree so that the plane wave based aggregation, translation and disaggregation procedures of FIAFTA can be utilized. As an alternative to the spherical harmonics expansion of Cartesian vector components of the plane wave spectra, it is also possible to work with TE and TM electromagnetic vector spherical harmonics expansions [9]. These need a larger number of expansion coefficients for small source boxes, but less for large source boxes [25]. In contrast to integral equation solutions as considered in [25], where the spherical harmonics expansion is used as an intermediate step, the spherical harmonics are directly utilized as the primary basis functions within FIAFTA. An NF transformation scenario with spherical harmonics spectral sources corresponding to the scenario in Fig. 4(a) is shown in Fig. 4(b). There are still spatial localization capabilities, but these are restricted by the chosen size of the source boxes. DUT and echo sources can still be treated separately.

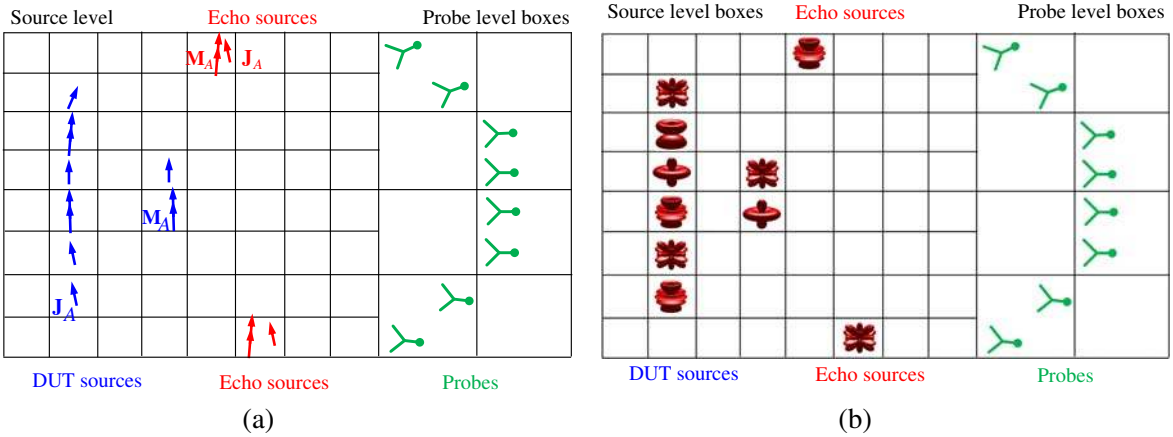

Figure 4. NF transformation scenario with (a) equivalent surface current densities, (b) spherical harmonics representation of the sources in a source box. In both cases, the sources are treated in boxes on the source level and the measurement probes are considered on a coarser level of the octree. DUT and echo sources can be separated in both cases due to spatial and spectral filtering.

[+] Please note that there is only one field expansion necessary, which comprises the fields of electric and magnetic sources.

5.4. Nonlinear Inverse Problems and Phaseless Field Transformations

In the preceding sections, focus was on the solution of linear inverse problems, i.e., the determination of equivalent sources from field observations. If only the amplitudes of the field observations are known and not the phases, the inverse problem becomes nonlinear and can, e.g., be written as [16, 17]

$$\min_{\mathbf{x}\in\mathbb{C}^N} f(\mathbf{x}), \quad f(\mathbf{x}) = \sum_{n=1}^{N_M} \frac{\left\|\mathbf{M}_n - \bar{\mathbf{C}}_n\,\mathbf{x}\circ\bar{\mathbf{C}}_n^*\,\mathbf{x}^*\right\|^2}{\left\|\mathbf{M}_n\right\|^2}, \tag{26}$$

where $f : \mathbb{C}^N \mapsto \mathbb{R}$, $\bar{\mathbf{C}}$ is the forward field transformation operator, $\mathbf{x}$ the vector of unknowns, $\mathbf{M}_n = \mathbf{b}_n \circ \mathbf{b}_n^*$ are the squared measurements, the subscript n indicates one set out of N_M sets of measurement samples[⋆] and $\circ$ is the Hadamard product. From this, it is clear that the linear FIAFTA transformations can be utilized as an efficient transformation operator within an appropriate nonlinear inverse problem solution, such as by the conjugate gradient algorithm. First results on this have been presented in [18] and are currently under further investigation.

Another type of nonlinear inverse problems, which can benefit from the flexibility and efficiency of the linear FIAFTA transformations, are nonlinear inverse medium problems, where the volumetric permittivity distribution within an imaging volume shall be determined from scattered field observations. Since the field observations are usually collected in some distance away from the actual imaging domain, it is possible to transform the field observations into equivalent surface current density distributions on a Huygens surface in close proximity to the actual imaging domain. This pre-processing step is a linear inverse equivalent surface current solution as discussed before in this paper, which can be performed by FIAFTA. For this kind of problem, it is, however, recommended to combine the inverse problem solution with a null-field condition for the interior of the Huygens surface in order to obtain Love equivalent surface current densities, which correspond directly to the tangential fields in the Huygens surface. These tangential fields can then be used as boundary conditions for a more localized nonlinear inverse problem solution. Initial investigations on this topic have been presented in [14, 15, 33].

6. NEAR-FIELD TRANSFORMATION RESULTS

The first scenario is a horn fed fan beam reflector antenna with a size of 60λ and with a TUM shaped slot of width 1λ, as shown in Fig. 5. The NF measurement data was computed by our MoM solver [25, 55] on a spherical measurement surface with a radius of 180λ assuming Hertzian dipoles as measurement probes. Next, the FIAFTA code according to Section 5.1 was utilized to compute equivalent surface current densities on the reflector geometry from the NF samples, where the information about the TUM shaped slot was, however, not put into the current expansion, i.e., surface current density basis functions were also assumed in the slot. The current distribution obtained from the inverse solution as shown in Fig. 5 demonstrates clearly the diagnostics capabilities of the FIAFTA code and the FF cut compared with the corresponding MoM results in Fig. 6(a) exhibits also excellent accuracy. In a second FIAFTA simulation with spherical harmonics sources within source level boxes with side length $\lambda/2$ (see Section 5.3), an even lower FF error[♯] compared to the MoM results was achieved, as seen in Fig. 6(b).

In the second example, true spherical NF measurements are considered, which have been obtained in the anechoic chamber of Technische Universität München with an open-ended waveguide probe for a measurement distance of about 2.75 m. The DUT is an R&S HF907 double-ridged waveguide horn specified for frequencies from 800 MHz to 18 GHz [56]. A picture of the antenna together with equivalent surface current densities on a Huygens surface around the antenna is shown in Fig. 7. The electric and magnetic surface current densities have been computed with FIAFTA according to Section 5.1 for a frequency of 18.0 GHz and they clearly illustrate the radiation behavior of the antenna. An even clearer insight into the NF distribution of the antenna is gained by the surface current densities shown in Fig. 8, which fulfill the Love condition in (4) and which have been obtained by postprocessing from the surface

[⋆] Measurement samples on different measurement surfaces, as often used for phaseless field transformations, are assigned to different sets.

[♯] The error level is computed by taking the linear difference of the magnitude of the fields and normalize it to the maximum of the reference field.

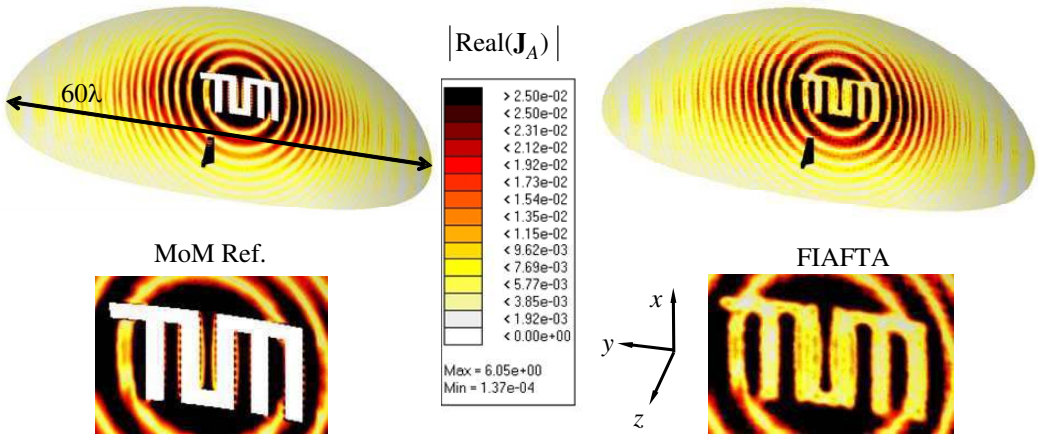

Figure 5. Horn fed fan beam reflector antenna with a 1λ wide slot in the form of the letters TUM standing for "Technische Universität München". Shown are electric surface current densities computed by a Method of Moments (MoM) solver [25, 55] and inverse equivalent surface current densities obtained from NF samples with the FIAFTA code. The NF samples were taken with Hertzian dipole probes on a spherical measurement surface with a radius of 180λ.

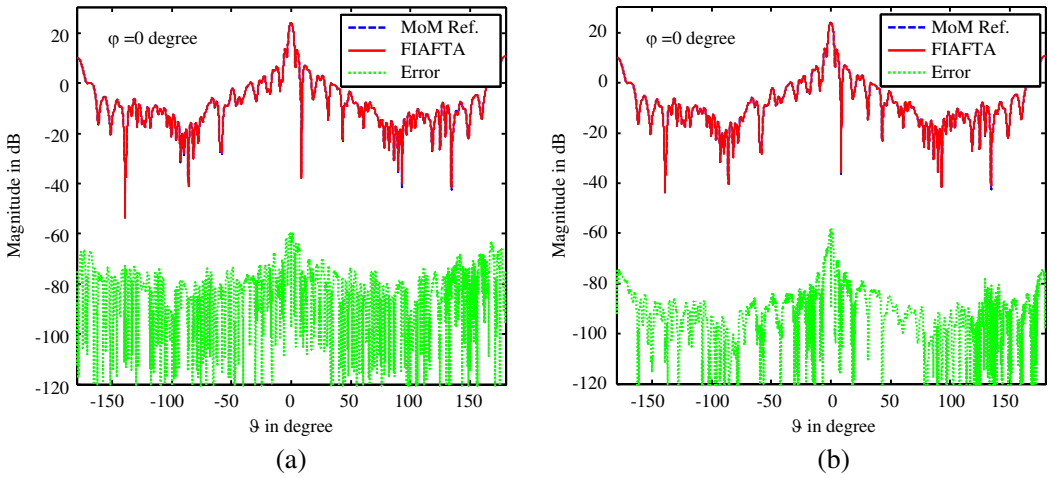

Figure 6. FF cuts obtained by FIAFTA for the fan beam reflector in Fig. 5 in comparison to MoM reference results: (a) FIAFTA with equivalent surface current densities on the reflector, (b) FIAFTA with spherical harmonics in source boxes with side length of $\lambda/2$.

current densities in Fig. 7. The triangular surface mesh representing the antenna comprises 188 090 triangles resulting in a total of 564 270 electric and magnetic surface current unknowns. The number of measurement points is 45 051, where two orthogonal polarizations were measured in every location. The computation time for one iteration of the inverse problem solution was here about 145 sec on one core of an Intel I7 processor with 3.7 GHz and a setup time of about 200 sec was required for the equivalent current computation. Running the same problem with spherical harmonics sources representing the antenna (see Section 5.3), defined in source boxes with a side length of $\lambda/2$, the setup time was reduced to about 55 sec, whereas the iteration time was similar as before. Dependent on the desired accuracy and the configuration of a problem, 5 to 80 iterations are usually sufficient to finalize the solution. Solving the problem with an algorithm utilizing regular sampling and global FFT based interpolation as well as separate octrees for the sources and the observation points resulted in an iteration time of about 56 sec on one core of the Intel I7 processor and of about 18 sec on four cores of the same processor.

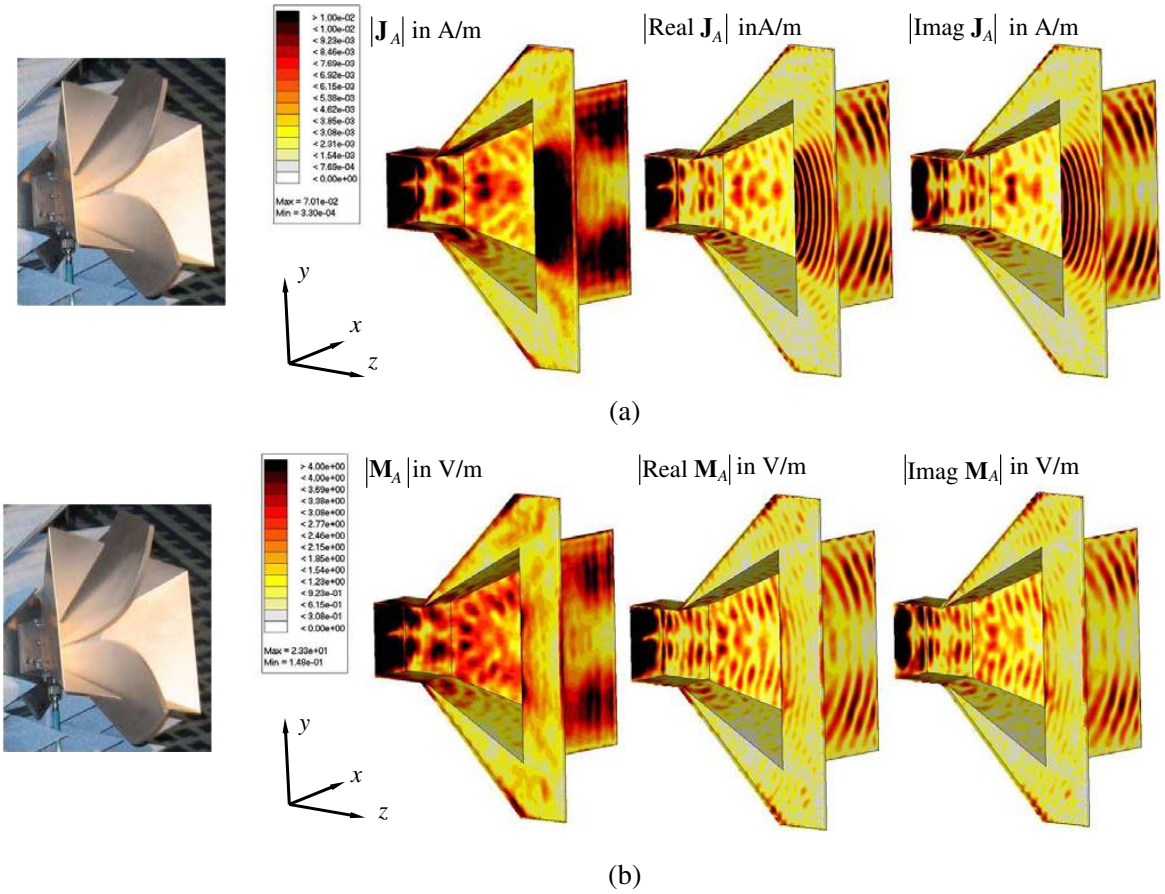

Figure 7. Photograph of R & S HF907 antenna [56] together with equivalent surface current densities obtained by FIAFTA from spherical NF measurements for a frequency of 18 GHz: (a) electric surface current density, (b) magnetic surface current density. Cut views of the assumed Huygens surface are shown.

For this solution spherical harmoncis expansion of the complete HF907 antenna was used. Co-polar and cross-polar H-plane and E-plane FF pattern cuts obtained from the two inverse problem solutions are depicted in Fig. 9 and in Fig. 10. The patterns are compared to the results obtained with the NSI NFFF transformation software [57] and it is seen that good agreement is achieved. The error levels are only shown for the FIAFTA spherical harmonics results. For the equivalent currents, the error with respect to the NSI results is slightly larger, since the equivalent current model enforces a more stringent spatial filtering than the spherical harmonics sources in FIAFTA and also in the NSI software. Fig. 11 illustrates finally a volumetric equivalent electric sources image, which has been computed from broadband measured data from $f = 8.0$ GHz to $f = 19$ GHz with a step size of 50 MHz. First, the near-fields were transformed into far-fields with the NSI transformation software and then the volumetric image was computed from the fully spherical plane wave spectra by hierarchical disaggregation as described in [32]. The images seen in the figure show orthogonal projections of the spatial volume current densities onto the outer surfaces of the cubical imaging domain. The active regions of the antenna can be clearly identified.

The next considered scenario is a scattering problem, where a plane wave is incident on a corner reflector as shown in Fig. 12. The NF samples assuming two perpendicular Hertzian dipole probes were again computed by our MoM solver in strongly irregular sample locations as also seen in Fig. 12. The incident plane wave was normally oriented with respect to the aperture of the triple reflector located in the plane $z = 577.5$ mm and the near-fields have been sampled in the plane $z = 1000$ mm with an average step size of $\lambda/2$ and an equally distributed random position variation in all three spatial directions with

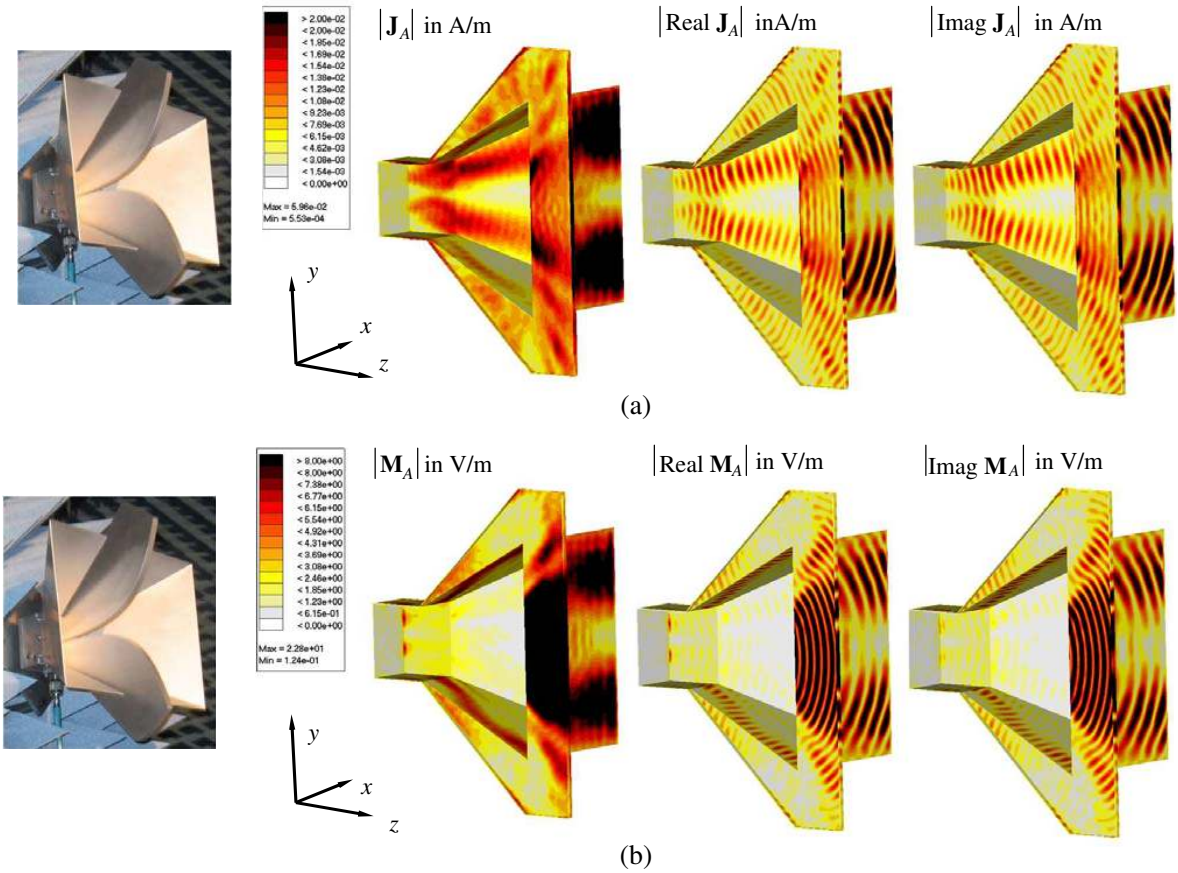

Figure 8. Love equivalent surface current densities for the configuration in Fig. 7: (a) electric surface current density, (b) magnetic surface current density. Cut views of the assumed Huygens surface are shown.

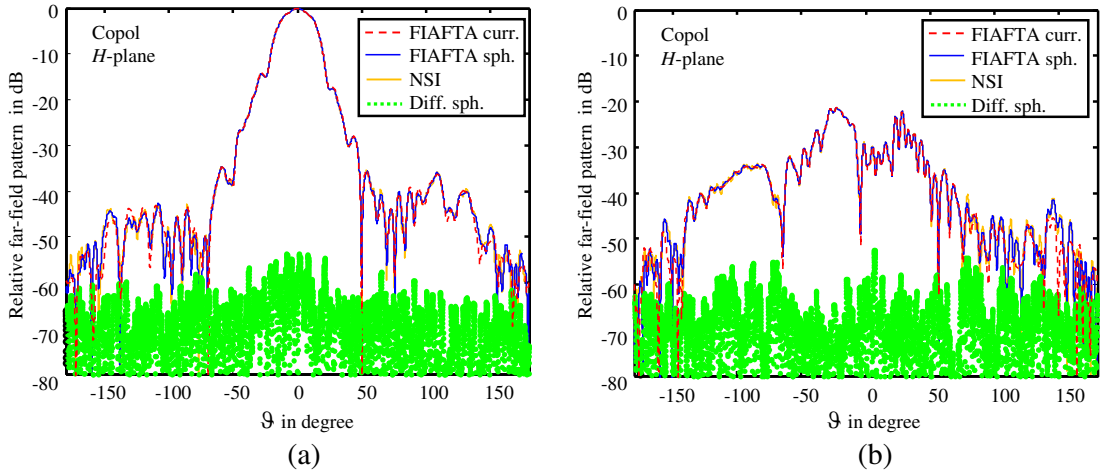

Figure 9. Normalized 18 GHz FF pattern H-plane cuts for the HF907 antenna in Fig. 7: FIAFTA results are shown in comparison to NSI results for equivalent surface current sources as illustrated in Fig. 7 and for spherical harmonics sources in boxes with $\lambda/2$ side length. The difference with respect to the NSI results is only shown for spherical harmonics sources.

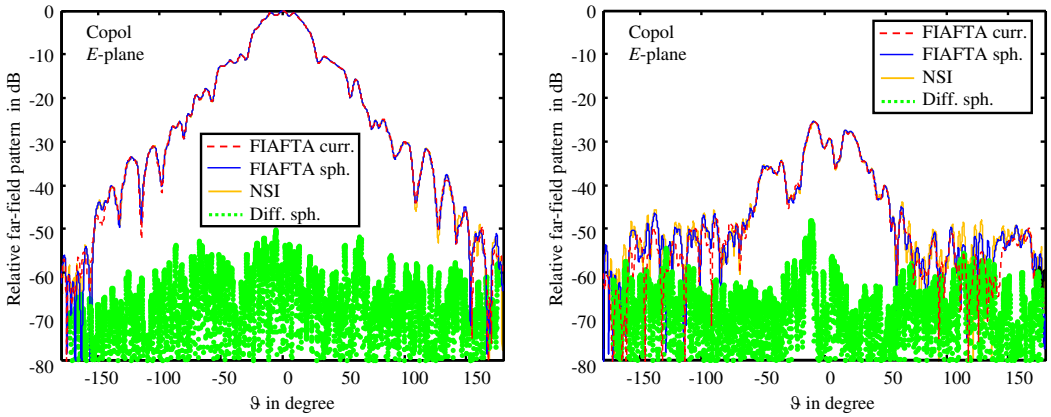

Figure 10. Normalized 18 GHz FF pattern E-plane cuts for the HF907 antenna in Fig. 7: FIAFTA results are shown in comparison to NSI results for equivalent surface current sources as illustrated in Fig. 7 and for spherical harmonics sources in boxes with $\lambda/2$ side length. The difference with respect to the NSI results is only shown for spherical harmonics sources.

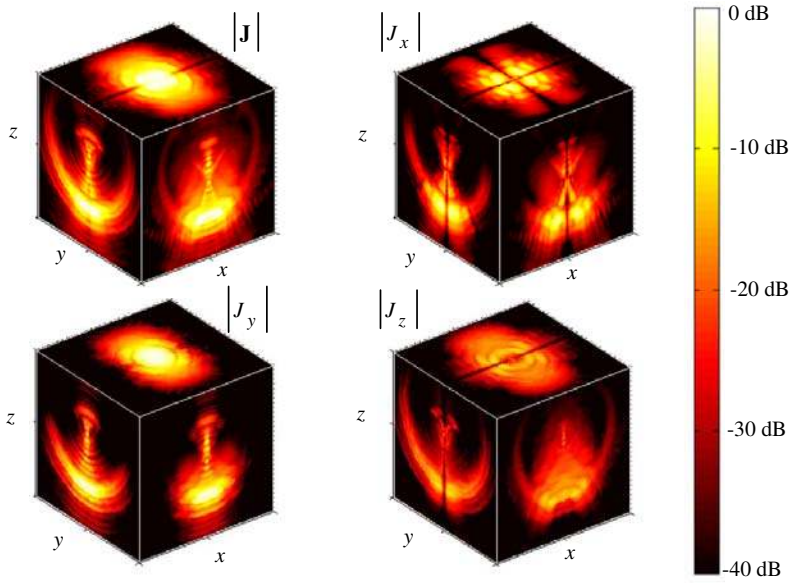

Figure 11. Volumetric image of the R & S antenna HF907 (see [56] and Fig. 7) obtained by hierarchical disaggregation and image formation from broadband FF data on the entire Ewald sphere. The FF data from $f = 8.0$ GHz to 19 GHz was obtained from NF measurements by spherical eigenmode based NFFF transformation with the NSI software [57].

an overall standard deviation of 0.707λ. The surface current density obtained with our MoM solver and 26 042 697 RWG unknowns is shown in Fig. 13(a) and the electric NF amplitude distribution in the 3 243 601 irregular sample locations according to Fig. 12[††] is depicted in Fig. 13(b). The inverse problem solution has been obtained with spherical harmonics expansion according to Section 5.3 (32 877 360 expansion coefficients in total) of the radiation fields of source boxes with side length $\lambda/2$ located in a plane above the aperture of the triple reflector. The computation time for one iteration of the inverse problem solution was about 2300 sec on one core of the Intel I7 processor with 3.7 GHz and a setup

[††] Only a few of the samples are seen.

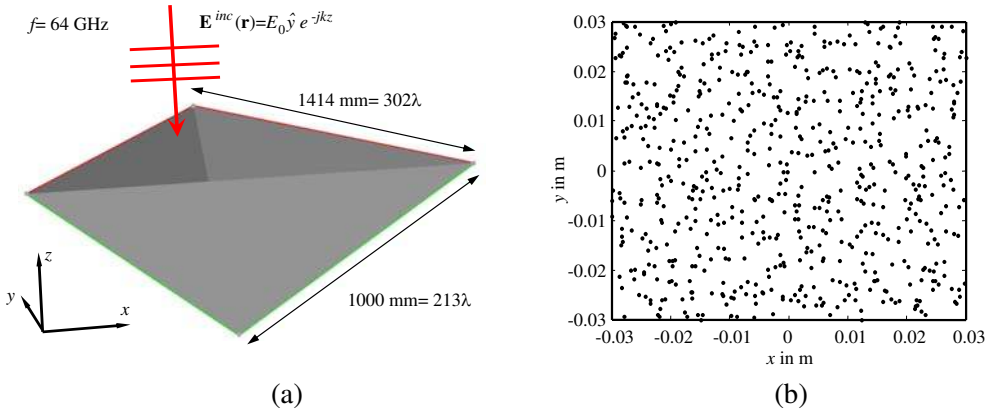

(a) (b)

Figure 12. Corner reflector with a normally incident plane wave, (a) geometry of the reflector, where the aperture is in the plane $z = 577.5$ mm, (b) illustration of the irregular sample locations in the plane $z = 1000$ mm.

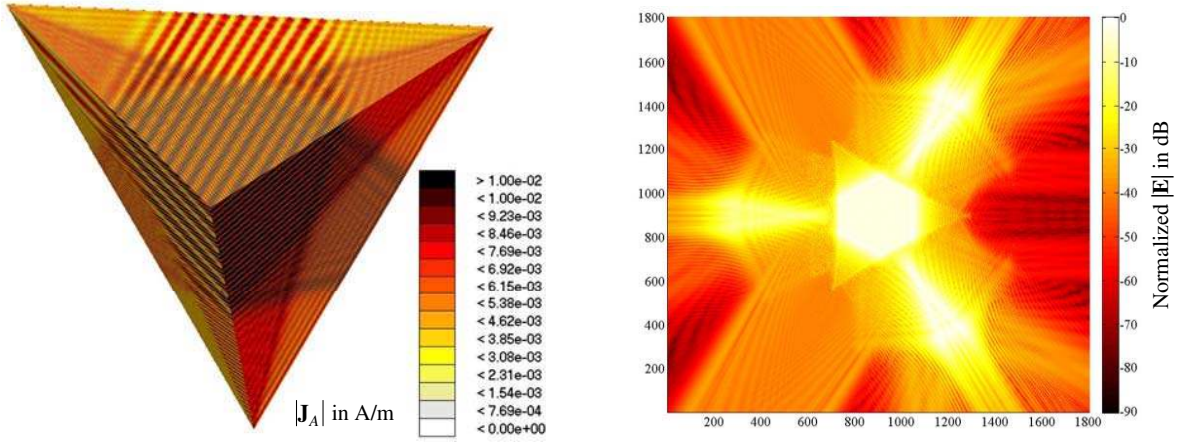

(a) (b)

Figure 13. (a) MoM surface current densities for the scattering configuration in Fig. 12, (b) electric NF amplitude in the irregular sample locations as illustrated in Fig. 12, obtained by our MoM solver, too.

time of about 200 sec was needed before the iterations could start. Utilizing the code with the global FFT based interpolation and the separate octrees, an iteration time of about 320 sec was achieved on 8 cores of an Intel Xeon X5690 processor with 3.47 GHz. A bistatic FF radar cross section (RCS) cut computed from the found spherical harmonics sources is compared to the MoM reference results in Fig. 14. Fig. 14(a) illustrates the wide angular validity of the transformed far-fields and shows also the achieved error level. Fig. 14(b) shows the same cut, but zoomed around the main peak. Additionally, it shows transformation results obtained with a standard 2D FFT based planar plane wave transformation algorithm as discussed in Section 3.1. For this transformation, the irregularly sampled field values were assumed to belong to a regular sample grid with step size $\lambda/2$ and it is interesting to note that the main peak and the first side lobes are still pretty well recovered.

The final example relates to the NFFF transformation of phaseless NF measurement data. We consider an aperture antenna of dimension 30 cm × 30 cm with its aperture located in the plane $y = 0.0$ m. Synthetic measurement data [58] with two perpendicular open-ended waveguide probes were generated in two measurement planes located at $y = -2.2$ m and at $y = -5.6$ m. The considered frequency was 5 GHz and equidistant sampling with a step size of $\lambda/4$ was performed, resulting into a total of 71 824 sample points. In order to test the robustness of the phaseless NFFF transformation, white Gaussian

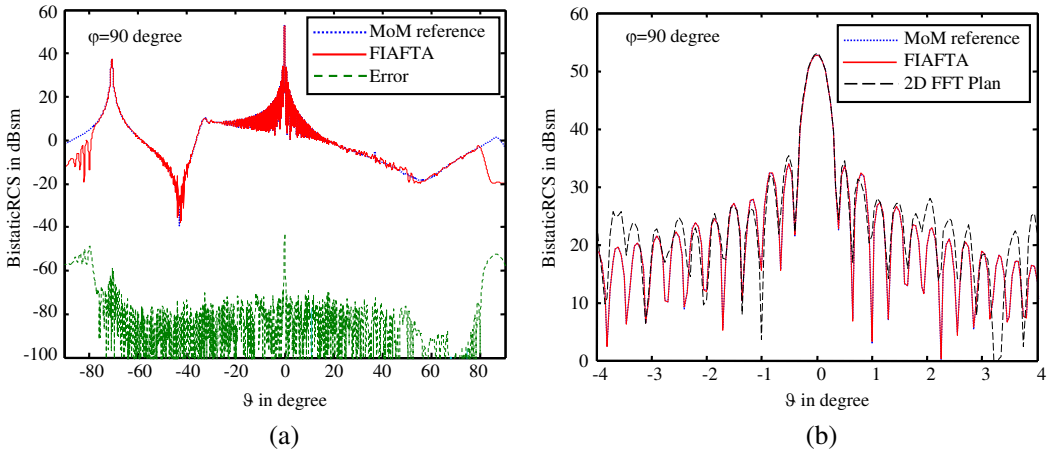

Figure 14. Radar cross section (RCS) cut obtained by the FIAFTA code for the corner reflector in Fig. 12: (a) complete cut with error level compared to MoM reference, (b) reduced angular range around the main peak and comparison with a standard 2D FFT based transformation result, where the sample locations have been assumed regular with $\lambda/2$ sample distance.

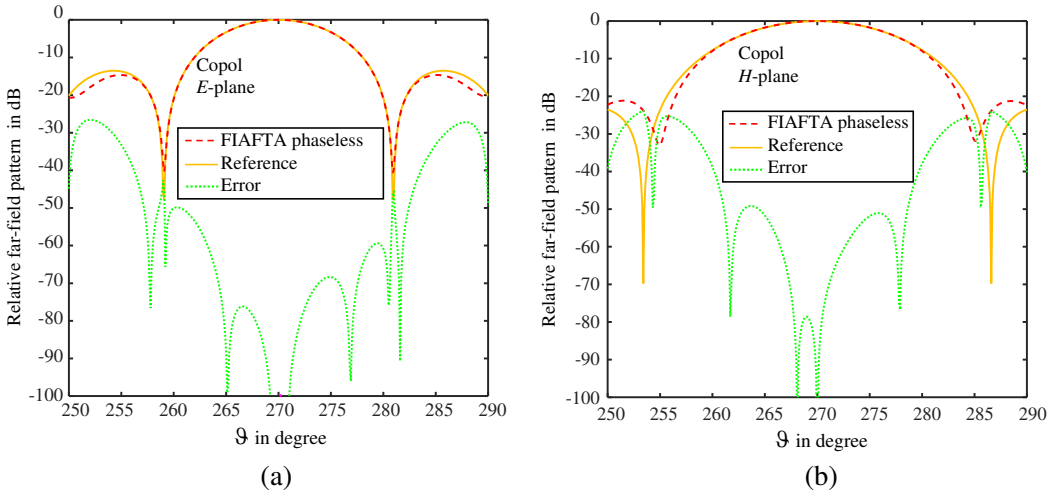

Figure 15. FF pattern cuts obtained from amplitude-only data: The considered DUT was an aperture antenna and open-ended rectangular waveguides were used as probes. The measurement and reference data was generated synthetically. The phaseless transformation was performed with the FIAFTA code combined with a nonlinear conjugate gradient solver as well as appropriate start vector estimation and updating [18, 19]. The measured data was corrupted by additive Gaussian noise with an SNR of 15 dB and the valid angle due to the planar measurement setup is about 20 degree. (a) E-plane cut, (b) H-plane cut.

noise according to a signal to noise ratio (SNR) of 15 dB was added to the measurement data. In the field transformation with FIAFTA, the test antenna was represented by spherical harmonics within a single source box (see Section 5.3). The linear FIAFTA transformation algorithm was combined with a nonlinear conjugate gradient solver [18, 19] and appropriate start vector estimation and updating in order to solve the nonlinear phaseless NFFF transformation problem. The estimated valid angle of the transformation according to the planar measurement setup is 20 degree in both cuts as shown in Fig. 15. Based on this and in view of the rather low SNR, the obtained transformation results are quite satisfying.

7. CONCLUSIONS

Electromagnetic field transformations are of importance for electromagnetic modelling and for electromagnetic field measurements with subsequent field transformations. It was shown that the basic field transformation equations are cumbersome to evaluate, and the consideration of a measurement probe antenna makes the problem even more involved. In many application fields, electromagnetic field transformation algorithms are based on eigenmode expansions of the pertinent Green's functions in order to realize very efficient transformation and even inversion algorithms by utilizing the orthogonality properties of the eigenmodes and by utilizing Fast Fourier Transformation (FFT) algorithms, which are, however, restricted to regular sampling of the field observations. Also, the orthogonality of the eigenmodes is only usable for field observations on canonical surfaces such as planes, cylinders and spheres. It was shown that efficient field transformation algorithms for irregular field observations or source distributions can be constructed by hierarchical multilevel approaches, where the field expansion with the purely propagating plane waves on the Ewald sphere has many advantages in this case, such as the possibility to work with diagonal translation operators. The Fast Irregular Antenna Field Transformation Algorithm (FIAFTA) is based on these concepts and it has many unique properties, which make it a flexible and efficient antenna and scattering field transformation approach for a wide variety of standard and specialized measurement tasks. FIAFTA supports arbitrarily located measurement samples and it has the ability to compensate arbitrary measurement probes. On the basis of an equivalent current formulation, it was shown that equivalent surface currents, plane wave spectra, and even spherical harmonics expansions can be used as unknowns for the inverse transformation problem to be solved by FIAFTA. The source grouping according to the hierarchical octree arrangement allows to consider spatial localization information for all three types of equivalent sources. The possibility to model scatterers or echoes by placing additional sources in the solution domain, gives the ability for an effective suppression of echo distortions. Various results were shown to demonstrate the capabilities of the fast irregular antenna field transformation algorithm.

ACKNOWLEDGMENT

The presented work has been supported in part by the European Space Agency (ESA) under ESA/ESTEC contracts ARTES 5.1: "Diagnostic Test Techniques for Trouble Shooting of Antennas During Satellite AIV"; Contract No. 21494/08/NL/ST and ARTES 34: "Portable Antenna Measurement System (PAMS) Prototype"; Contract No. 4000101551/10/NL/AD as well as by Deutsche Forschungsgemeinschaft (DFG) under grant Ei 352/16-1.

REFERENCES

1. Maxwell, J. C., "A dynamical theory of the electromagnetic field," *Philosophical Transactions of the Royal Society of London*, 459–512, 1865 (First presented to the British Royal Society in 1864).
2. Kong, J. A., *Electromagnetic Wave Theory*, 2nd Edition, John Wiley & Sons, New York, 1990.
3. Balanis, C. A., *Antenna Theory and Design*, John Wiley & Sons, Hoboken, 2005.
4. Jin, J.-M., *Theory and Computation of Electromagnetic Fields*, Wiley-IEEE Press, Hoboken, 2010.
5. Carson, J. R., "Reciprocal theorems in radio communications," *Proc. IRE*, Vol. 17, 952–956, Jun. 1929.
6. Rumsey, V. H., "Reaction concept in electromagnetic theory," *Physical Review*, Vol. 94, No. 6, 1484–1494, 1954.
7. Richmond, J. H., "A reaction theorem and its application to antenna impedance calculation," *IRE Trans. on Antennas and Propag.*, 515–520, Nov. 1961.
8. Harrington, R.-F., *Field Computation by Moment Methods*, IEEE Press, Piscataway, 1992.
9. Chew, W. C., J.-M. Jin, E. Michielssen, and J. Song, *Fast and Efficient Algorithms in Computational Electromagnetics*, Artech House Publishers, 2001.
10. Ylä-Oijala, P., "Calculation of CFIE impedance matrix elements with RWG and n $\times$ RWG functions," *IEEE Trans. on Antennas and Propag.*, Vol. 51, No. 8, 1837–1846, 2003.

11. Li, L. and T. F. Eibert, "A projection height independent adaptive radial-angular-R^2 transformation for singular integrals," *IEEE Trans. on Antennas and Propag.*, Vol. 62, No. 10, 5381–5386, 2014.
12. Araque Quijano, J. L. and G. Vecchi, "Field and source equivalence in source reconstruction on 3D surfaces," *Progress In Electromagnetics Research*, Vol. 103, 67–100, 2010.
13. Jorgensen, E., P. Meincke, and C. Cappellin, "Advanced processing of measured fields using field reconstruction techniques," *European Conference on Antennas and Propagation*, 3880–3884, Rome, Apr. 2011.
14. Kılıç, E. and T. F. Eibert, "A three-dimensional microwave imaging technique combining inverse equivalent current and finite element methods," *XXXI URSI General Assembly and Scientific Symposium*, Beijing, China, Aug. 2014.
15. Kılıç, E. and T. F. Eibert, "Solution of 3D inverse scattering problems by combined inverse equivalent current and finite element methods," *Journal of Computational Physics*, Vol. 288, 131–149, 2015.
16. Bucci, O. V., G. d'Elia, G. Leone, and R. Pierri, "Far-field pattern determination from the near-field amplitude on two surfaces," *IEEE Trans. on Antennas and Propag.*, Vol. 38, No. 11, 1772–1779, 1990.
17. Isernia, T., G. Leone, and R. Pierri, "Radiation pattern evaluation from near-field intensities on planes," *IEEE Trans. on Antennas and Propag.*, Vol. 44, No. 5, 701–710, 1996.
18. Schnattinger, G., C. Lopez, E. Kılıç, and T. F. Eibert, "Fast near-field far-field transformation for phaseless and irregular antenna measurement data," *Advances in Radio Science*, Vol. 12, 171–177, 2014.
19. Lopez, C., R. A. M. Mauermayer, and T. F. Eibert, "Extending the plane wave based fast irregular antenna field transformation algorithm for amplitude-only data, *European Conference on Antennas and Propagation*, Lisbon, Portugal, Apr. 2015.
20. Yaghjian, A. D., "An overview of near-field antenna measurements," *IEEE Trans. on Antennas and Propag.*, Vol. 34, No. 1, 30–45, 1986.
21. Alvarez, Y., F. Las-Heras, and M. R. Pino, "Reconstruction of equivalent currents distribution over arbitrary three-dimensional surfaces based on integral equation algorithms," *IEEE Trans. on Antennas and Propag.*, Vol. 55, No. 12, 3460–3468, 2007.
22. Eibert, T. F. and C. H. Schmidt, "Multilevel fast multipole accelerated inverse equivalent current method employing Rao-Wilton-Glisson discretization of electric and magnetic surface currents," *IEEE Trans. on Antennas and Propag.*, Vol. 57, No. 4, 1178–1185, 2009.
23. Eibert, T. F., Ismatullah, E. Kaliyaperumal, and C. H. Schmidt, "Inverse equivalent surface current method with hierarchical higher order basis functions, full probe correction and multilevel fast multipole acceleration," *Progress In Electromagnetics Research*, Vol. 106, 377–394, 2010.
24. Petre, P. and T. K. Sarkar, "Planar near-field to far-field transformation using an equivalent magnetic current approach," *IEEE Trans. on Antennas and Propag.*, Vol. 40, No. 11, 1348–1356, 1992.
25. Eibert, T. F., "A diagonalized multilevel fast multipole method with spherical harmonics expansion of the k-space integrals," *IEEE Trans. on Antennas and Propag.*, Vol. 53, No. 2, 814–817, 2005.
26. Alvarez, Y., F. Las-Heras, M. R. Pino, and J. A. Lopez, "Acceleration of the sources reconstruction method via the fast multipole method," *IEEE Antennas Propag. Intern. Symp.*, San Diego, CA, 2008.
27. Schmidt, C. H., M. M. Leibfritz, and T. F. Eibert, "Fully probe-corrected near-field far-field transformation employing plane wave expansion and diagonal translation operators," *IEEE Trans. on Antennas and Propag.*, Vol. 56, No. 3, 737–746, 2008.
28. Schmidt, C. H. and T. F. Eibert, "Multilevel plane wave based near-field far-field transformation for electrically large antennas in free-space or above material halfspace, *IEEE Trans. on Antennas and Propag.*, Vol. 57, No. 5, 1382–1390, 2009.

29. Qureshi, M. A., C. H. Schmidt, and T. F. Eibert, "Adaptive sampling in multilevel plane wave based near-field far-field transformed planar near-field measurements," *Progress In Electromagnetic Research*, Vol. 126, 481–497, 2012.
30. Qureshi, M. A., C. H. Schmidt, and T. F. Eibert, "Efficient near-field far-field transformation for nonredundant sampling representation on arbitrary surfaces in near-field antenna measurements," *IEEE Trans. on Antennas and Propag.*, Vol. 61, No. 4, 2025–2033, 2013.
31. Yinusa, K. and T. F. Eibert, "A multi-probe antenna measurement technique with echo suppression capability," *IEEE Trans. on Antennas and Propag.*, Vol. 61, No. 10, 5008–5016, 2013.
32. Schnattinger, G. and T. F. Eibert, "Solution to the full vectorial 3D inverse source problem by multi-level fast multipole method inspired hierarchical disaggregation," *IEEE Trans. on Antennas and Propag.*, Vol. 60, No. 7, 3325–3335, 2012.
33. Kılıç, E. and T. F. Eibert, "An inverse scattering technique based on finite element — Boundary integral method," *Progress In Electromagnetics Research Symposium Abstracts*, 777, Stockholm, Sweden, Aug. 12–15, 2013.
34. Qureshi, M. A., C. H. Schmidt, and T. F. Eibert, "Near-field error analysis for arbitrary scanning grids using fast irregular antenna field transformation algorithm," *Progress In Electromagnetics Research B*, Vol. 48, 197–220, 2013.
35. Schnattinger, G., R. A. M. Mauermayer, and T. F. Eibert, "Monostatic radar cross section near-field far-field transformations by multilevel plane wave decomposition," *IEEE Trans. on Antennas and Propag.*, Vol. 62, No. 8, 4259–4268, 2014.
36. Fritzel, T., A. Geise, C. H. Schmidt, H.-J. Steiner, T. F. Eibert, O. Wiedenmann, and M. Paquay, "Concept of a portable antenna measurement system for large-scale and multi-contour near-field measurements," *35th ESA Antenna Workshop on Antenna and Free Space RF Measurements, ESA/ESTEC*, Noordwijk, The Netherlands, 2013.
37. Bucci, O. M. and G. Franceschetti, "On the spatial bandwidth of scattered fields," *IEEE Trans. on Antennas and Propag.*, Vol. 35, No. 12, 1445–1455, 1987.
38. Bucci, O. M., C. Gennarelli, and C. Savarese, "Representation of electromagnetic fields over arbitrary surfaces by a finite and nonredundant number of samples," *IEEE Trans. on Antennas and Propag.*, Vol. 46, No. 3, 351–359, 1998.
39. Bucci, O. M. and C. Gennarelli, "Application of nonredundant sampling representation of electromagnetic fileds to NF-FF transformation techniques," *International Journal of Antennas and Propagation*, Vol. 2012, 1–14, 2011.
40. Gregson, S., J. McCormick, and C. Parini, *Principles of Planar Near-field Antenna Measurements*, IET Electromagnetic Waves, UK, 2007.
41. Hansen, J., *Spherical Near-field Antenna Measurements*, IEEE Electromagnetic Wave Series 26, UK, 1988.
42. Laitinen, T., S. Pivnenko, J. M. Nielsen, and O. Breinbjerg, "Theory and practice of the FFT/matrix inversion technique for probe-corrected spherical near-field antenna measurements with higher-order probes," *IEEE Trans. on Antennas and Propag.*, Vol. 58, No. 8, 2623–2631, 2010.
43. Hansen, T. B., "Spherical near-field scanning with higher-order probes," *IEEE Trans. on Antennas and Propag.*, Vol. 59, No. 11, 4049–4059, 2011.
44. Hansen, T. B., "Exact Gaussian-beam theory for outgoing and standing spherical waves: Application to transmitting and receiving antennas," *IEEE Trans. on Antennas and Propag.*, Vol. 60, No. 3, 1291–1302, 2012.
45. Chew, W. C., T. J. Cui, and J. M. Song, "A FAFFA-MLFMA algorithm for electromagnetic scattering," *IEEE Trans. on Antennas and Propag.*, Vol. 50, No. 11, 1641–1649, 2002.
46. Cui, T. J., W. C.Chew, G. Chen, and J. M. Song, "Efficient MLFMA, RPFMA, and FAFFA algorithms for EM scattering by very large structures," *IEEE Trans. on Antennas and Propag.*, Vol. 52, No. 3, 759–770, 2004.

47. Hansen, T. B., "Translation operator based on Gaussian beams for the fast multipole method in three dimensions," *Wave Motion*, Vol. 50, 940–954, 2013.
48. Tzoulis, A. and T. F. Eibert, "Efficient electromagnetic near-field computation by the multilevel fast multipole method employing mixed near-field/far-field translations," *IEEE Antennas and Wireless Propagation Letters*, Vol. 4, 449–452, 2005.
49. Eibert, T. F., "A multilevel fast spectral domain algorithm for electromagnetic analysis of infinite periodic arrays with large unit cells," *Advances in Radio Science*, Vol. 4, 111–115, 2006.
50. Björck, A., *Numerical Methods for Least Squares Problems,* SIAM, Philadelphia, 1996.
51. Saad, Y., *Iterative Methods for Sparse Linear Systems,* PWS, Boston, 1996.
52. Sarvas, J., "Performing interpolation and anterpolation entirely by fast Fourier transform in the 3-D multilevel fast multipole algorithm," *SIAM J. Numer. Anal.*, Vol. 41, No. 6, 2180–2196, 2003.
53. Järvenpää, S. and P. Ylä-Oijala, "A global interpolator with low sample rate for multilevel fast multipole algorithm," *IEEE Trans. on Antennas and Propag.*, Vol. 61, No. 3, 1291–1300, 2013.
54. Järvenpää, S. and P. Ylä-Oijala, "Multilevel fast multipole algorithm with global and local interpolators," *IEEE Trans. on Antennas and Propag.*, Vol. 62, No. 9, 4716–4725, 2014.
55. Eibert, T. F., "Some scattering results computed by the hybrid finite element — Boundary integral — Multilevel fast multipole method," *IEEE Antennas and Propag. Magazine*, Vol. 49, No. 2, 61–69, Apr. 2007.
56. Rohde & Schwarz, "Double ridged waveguide antenna," http://www.rohde-schwarz.de/product/hf907.html.
57. Nearfield Systems Inc., "Antenna measurement solutions," www.nearfield.com.
58. Schmidt, C. H., D. T. Schobert, and T. F. Eibert, "Electric dipole based synthetic data generation for probe-corrected near-field antenna measurements," *European Conference on Antennas and Propagation*, 3269–3273, 2011.